J. Fluid Mech. (1984), *vol.* 146, *pp.* 21–43
Printed in Great Britain

The emergence of isolated coherent vortices in turbulent flow

By JAMES C. McWILLIAMS
National Center for Atmospheric Research, Boulder, Colorado 80307

(Received 7 September 1983 and in revised form 16 April 1984)

A study is made of some numerical calculations of two-dimensional and geostrophic turbulent flows. The primary result is that, under a broad range of circumstances, the flow structure has its vorticity concentrated in a small fraction of the spatial domain, and these concentrations typically have lifetimes long compared with the characteristic time for nonlinear interactions in turbulent flow (i.e. an eddy turnaround time). When such vorticity concentrations occur, they tend to assume an axisymmetric shape and persist under passive advection by the large-scale flow, except for relatively rare encounters with other centres of concentration. These structures can arise from random initial conditions without vorticity concentration, evolving in the midst of what has been traditionally characterized as the 'cascade' of isotropic, homogeneous, large-Reynolds-number turbulence: the systematic elongation of isolines of vorticity associated with the transfer of vorticity to smaller scales, eventually to dissipation scales, and the transfer of energy to larger scales. When the vorticity concentrations are a sufficiently dominant component of the total vorticity field, the cascade processes are suppressed. The demonstration of persistent vorticity concentrations on intermediate scales – smaller than the scale of the peak of the energy spectrum and larger than the dissipation scales – does not invalidate many of the traditional characterizations of two-dimensional and geostrophic turbulence, but I believe it shows them to be substantially incomplete with respect to a fundamental phenomenon in such flows.

1. Introduction

The dynamics of large-scale, extratropical, planetary fluid motions are usually approximately geostrophic, and hence nearly horizontally non-divergent and approximately two-dimensional in this sense, as well as only weakly non-conservative. In these circumstances most phenomena can be interpreted as hybrids of several dynamical regimes, at least away from boundaries: dispersive Rossby waves, geostrophic or two-dimensional turbulence, and isolated, coherent vortices. Usually the regime boundaries can be identified by simple scale arguments. If phase speeds are greater than fluid-particle speeds, then wave processes are likely to be dominant. Isolated, coherent (i.e. long-lived) vortices, with the appropriate structure to be a self-consistent solution in an otherwise quiescent fluid, are likely to persist if their particle speeds are larger than those of any disorderly flow structures in their neighbourhood (McWilliams *et al.* 1981; Malanotte-Rizzoli 1982). If these conditions are not met, then a turbulent interpretation is usually made, at least for the transient component of the flow. Turbulence, of course, has many, not wholly consistent, definitions, but short persistence times for any particular flow configuration (of the order of a particle recirculation time or 'eddy turnaround time') and limited predictability from imperfectly known initial or boundary conditions are often

essential characteristics. The term 'cascade' is often used to indicate the strong nonlinear interactions between quite disparate scales of motion which can account for these characteristics.

This paper is a report of numerical solutions which demonstrate that isolated coherent vortices can coexist with and evolve out of actively cascading turbulence, even when there are no gross scale differences between the two components of the flow. Parts of this demonstration have been made previously in the numerical studies of Fornberg (1977) and Basdevant *et al.* (1981). Most attention here will be directed to the simplest and most extensively studied example of geostrophic turbulence – the slow frictional decay of isotropic, homogeneous, two-dimensional turbulence. This latter problem, of course, also has an extensive history of investigation outside of the context of planetary fluid dynamics (e.g. Batchelor 1953; Kraichnan & Montgomery 1980). However, the occurrence of isolated vortices is much more general than just in decaying two-dimensional turbulence. In support of this, several examples of more general geostrophic-turbulence solutions will also be described.

2. The model

A set of model equations which is sufficiently general to encompass all calculations to be reported here is the non-dimensional, equivalent-barotropic, quasigeostrophic, β-plane, potential-vorticity balance with forcing and various types of damping:

$$\left.\begin{aligned} \frac{\partial}{\partial t}(\zeta-\gamma^2\psi)+\mathrm{J}(\psi,\zeta-\gamma^2\psi+\beta y) &= f-\nu_0\zeta+\nu_2\nabla^2\zeta-\nu_4\nabla^4\zeta, \\ \zeta=\nabla^2\psi, \quad u=-\frac{\partial\psi}{\partial y}, \quad v&=\frac{\partial\psi}{\partial x}. \end{aligned}\right\} \tag{1}$$

x, y and t are East, North and time coordinates, ψ is the stream function, u and v are the East and North velocities and ζ is the vorticity. γ is the inverse of the radius of deformation, β is the northward gradient of the Coriolis frequency, f is the forcing function, and the ν_i are damping coefficients – referred to as Rayleigh friction, Newtonian viscosity and hyperviscosity for $i = 0$, 2 and 4. J is the Jacobian operator in x and y.

We shall examine a simple special case of (1) in particular detail; viz decaying two-dimensional flow:

$$\left.\begin{aligned} \gamma=\beta=f=\nu_0=\nu_2&=0, \\ \frac{\partial\zeta}{\partial t}+\mathrm{J}(\psi,\zeta)&=-\nu_4\nabla^4\zeta. \end{aligned}\right\} \tag{2}$$

The choice of hyperviscosity is dictated by a desire to confine the effects of damping to the smallest resolved scales of the model, leaving the more energetic scales nearly inviscid. The traditional formulation of decaying two-dimensional flow includes Newtonian viscosity in place of hyperviscosity in (2). Solutions of the two differently formulated problems do not differ in any important manner in the properties discussed in §§3–5 below. However, for a fixed numerical resolution a higher effective Reynolds number is achievable with hyperviscosity, and for this reason (2) is given the great attention, while its Newtonian viscosity counterpart is more briefly reported in §6.

These equations are solved as an initial-value problem in a doubly periodic square domain of width 2π. The numerical model is a dealiased, pseudospectral (Fourier

expansion) one with approximately circular truncation in the horizontal wavenumber plane. It conserves area averages of both energy and potential enstrophy,

$$\left.\begin{aligned} E &\equiv \frac{1}{2}\frac{1}{(2\pi)^2}\iint \mathrm{d}x\,\mathrm{d}y\,(u^2+v^2), \\ V &\equiv \frac{1}{(2\pi)^2}\iint \mathrm{d}x\,\mathrm{d}y\,(\zeta-\gamma^2\psi)^2, \end{aligned}\right\} \tag{3}$$

when the forcing and damping terms are zero. Properties of the model are more fully described in Haidvogel (1983); it is an extension of an earlier model described in Davey (1980).

3. Decaying two-dimensional flow

The initial conditions for (2) are a Gaussian random realization for each Fourier component of ψ, where at each vector wavenumber the ensemble variance is proportional to the prescribed scalar wavenumber function

$$k^{-1}\left[1+\left(\frac{k}{k_0}\right)^4\right]^{-1}, \quad k>0, \tag{4}$$

where k is the wavenumber-vector magnitude. This function is broadband and peaked near wavenumber k_0. The amplitude factor is chosen such that $E = 0.5$ initially. The resulting kinetic-energy spectrum is shown in figure 2, for $k_0 = 6$, where $E(k)$ is defined as the sum of the kinetic-energy density for all model wavenumber vectors whose magnitude lies within a band of width $\Delta k = 1$ centred on integer k-values. (Because the domain size is 2π, each component of the wavenumber vector assumes all integer values with magnitudes bounded by the truncation level N.) This definition implies

$$E = \sum_{k=1}^{N} E(k). \tag{5}$$

The value selected for N is approximately 128, corresponding to $NG = 256$ spatial grid points in each direction. The value selected for the hyperviscosity is 3.125×10^{-8}, which, because of the domain size and E-value, can be interpreted as an inverse Reynolds number for the largest scales (it is not, of course, isomorphic to a Reynolds number constructed from Newtonian viscosity). This implies a very slow rate of energy decay, as is shown in figure 1*a*.

Time series for E, V and the energy centroid wavenumber

$$\bar{k} \equiv E^{-1}\sum_{k} kE(k) \tag{6}$$

are plotted in figure 1. The energy decay rate is indeed small, with less than a 3% decrease over a time of 40 units, where a unit is approximately a recirculation time for eddies of the most energetic scale. More precisely, we define an eddy turnaround time τ_{E} as either $2\pi V^{-\frac{1}{2}}$ or $2\pi(2E)^{-\frac{1}{2}}\bar{k}^{-1}$; the former has values that increase from 0.5 to 2.0 as the solution evolves, and the latter has values about 50% larger. The enstrophy-decay rate, however, is initially quite substantial – in contrast with the energy rate, it is expected to remain finite as the hyperviscosity tends to zero – although it slows considerably after a few τ_{E}. The centroid wavenumber decreases monotonically with time – energy is transferred to larger scales – although its rate also slows with time. Figure 2 shows that the energy spectra change rapidly in the first few τ_{E},

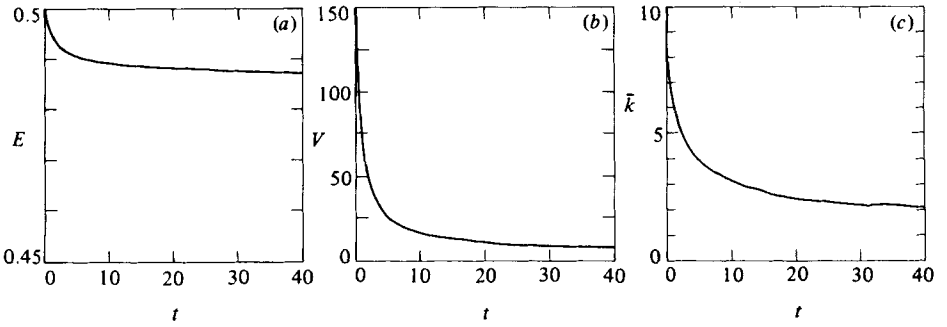

FIGURE 1. Time series of E, V and $\bar{k}$.

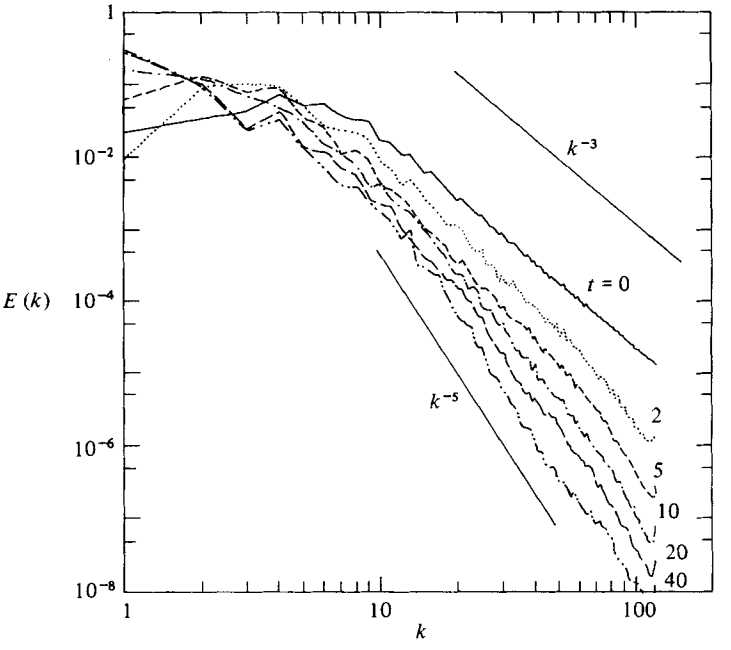

FIGURE 2. $E(k)$ at $t = 0$, 2, 5, 10, 20 and 40.

primarily by steepening at large k from the initial shape of k^{-3}. Subsequently $E(k)$ undergoes little change in shape, except for weak fluctuations in the small-k components and a slow decrease in all components which is somewhat greater at larger k. Plots of ψ (figure 3) also exhibit a systematic evolution towards larger scales. All of these properties are familiar ones from previous investigations of decaying two-dimensional turbulence.

A much less familiar property is illustrated in figure 4. The vorticity field evolves from an initially fairly uniform distribution in space to a collection of discrete and usually isolated vorticity extrema. These isolated vortices occur with a variety of amplitudes and sizes, although all of them are substantially smaller in size than the dominant stream-function patterns. Most of them are approximately axisymmetric, but there are obvious exceptions when two or more of them are close enough to interact strongly. The interactions are of several types, all of which are represented in figure 4: a weaker vortex can be engulfed (if of the same sign) or sheared out if

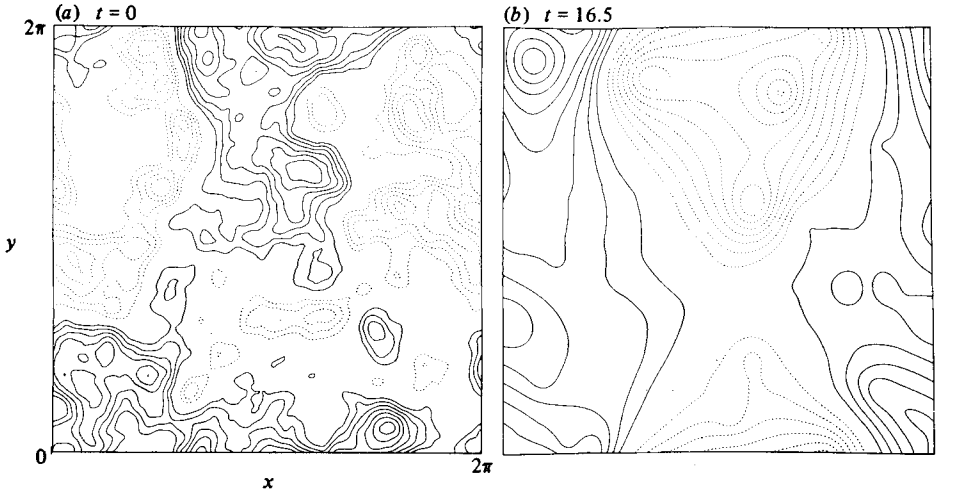

FIGURE 3. Stream function at $t = 0$ and 16.5. The contour intervals are 0.1 and 0.2 respectively. Positive contours are solid and negative dashed; the zero contour has been deleted.

it approaches a stronger vortex too closely; in other cases a close approach leads to strong deformations of vorticity contours followed by relaxation towards axisymmetry after separating; vortices of comparable strength but opposite sign can become attached to each other, much like a modon, and consequently undergo rapid movement through the fluid, until some other close encounter tears them apart. The enormous qualitative difference between the distributions of ψ and ζ is expressed by the kurtosis calculated in an average over all spatial grid-point values at fixed t (figure 5): stream function remains close to the Gaussian value of 3, while vorticity departs from it monotonically owing to the disappearance of vorticity in the space between and the persistence of vorticity within the isolated vortices. The high kurtosis reflects a particular kind of spatial and temporal intermittency. Intermittency in general is an explanation of spectrum shapes steeper than the inertial-range form k^{-3} (Basdevant *et al.* 1981), such as those in figure 2, although, even without intermittency, spectra can be steeper than k^{-3} owing to finite resolution and dissipation.

A geometric interpretation of large kurtosis is the following. If a two-dimensional field consists of elemental structures of compact support, which are non-zero only within squares of breadth a separated by a distance b, then the kurtosis is proportional to $(b/a)^2$. The kurtosis is large whenever the separation distance is large compared with the breadth of the structures. This condition holds approximately in figures 4 (c, d).

The properties shown in figures 4 and 5 are surprising, certainly to me, and I suspect to others as well. The distributions in figure 4 can be contrasted with one or more 'typically turbulent' (figure 6). It is from an equilibrium two-dimensional flow solution which is sufficiently strongly forced and damped so that no vorticity concentrations or non-Gaussian kurtosis develop (equilibrium solutions are discussed further in §6). The vorticity pattern in this case has the elongated contours which are often taken to be the signature of cascading two-dimensional turbulence (Batchelor 1969).

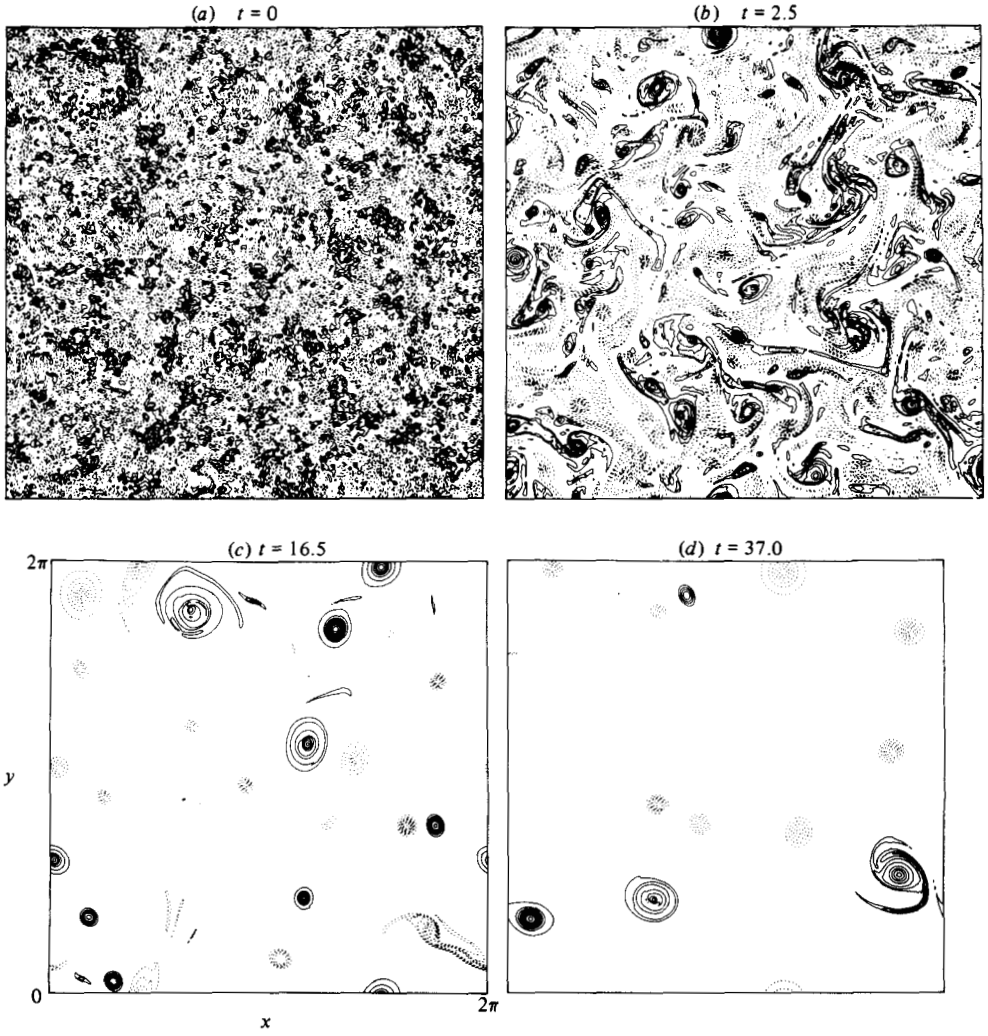

FIGURE 4. Vorticity at $t = 0$, 2.5, 16.5 and 37. The contour interval is 8 for the first of these and 4 thereafter. The line coding is as in figure 3.

4. A description of how isolated vortices emerge and persist

This section contains a description of what happens to vorticity extrema in the preceding decay solution. The basis for it is a sequence of maps like those in figure 4, too many to be included here in their entirety.

Each vortex in figure 4 (*b–d*), with a magnitude of at least three contours, can be traced backwards in time, without interruption, to the initial conditions. That is, throughout its history it is an identifiable, localized vorticity concentration which is never distorted too far from an axisymmetric distribution. The converse is not true. Individual vortices can cease to be traceable through interactions with other, generally stronger vortices, during which they are either destroyed by being sheared to the point of participating in a local turbulent cascade or absorbed into the stronger vortex. A necessary condition for absorption, or merger, is that they both have the same sign of vorticity. In the initial conditions, the incipient isolated vortices are local

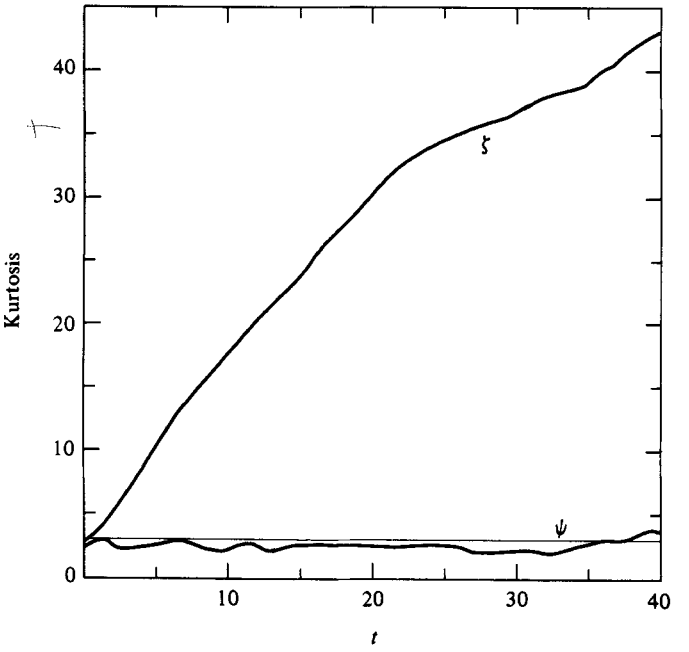

FIGURE 5. Kurtosis for stream function and vorticity.

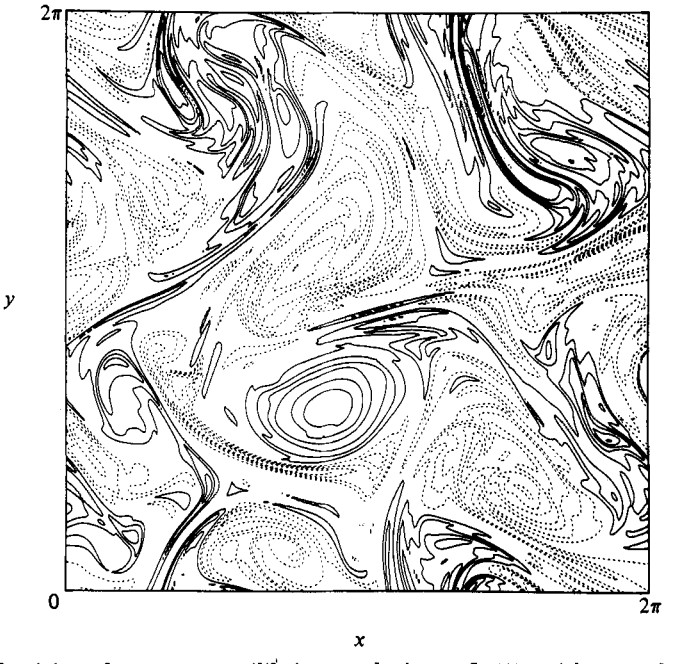

FIGURE 6. Vorticity from an equilibrium solution of (1) with $\gamma = \beta = \nu_2 = 0$, $\nu_0 = 0.1$, $\nu_4 = 5 \times 10^{-8}$, and f a random forcing which is white noise in time and isotropic in space with non-zero amplitude only for k-values between 1 and 4. The plotting convention is as in figure 4 except that the contour interval is reduced to 1 owing to the somewhat smaller E and V in this solution.

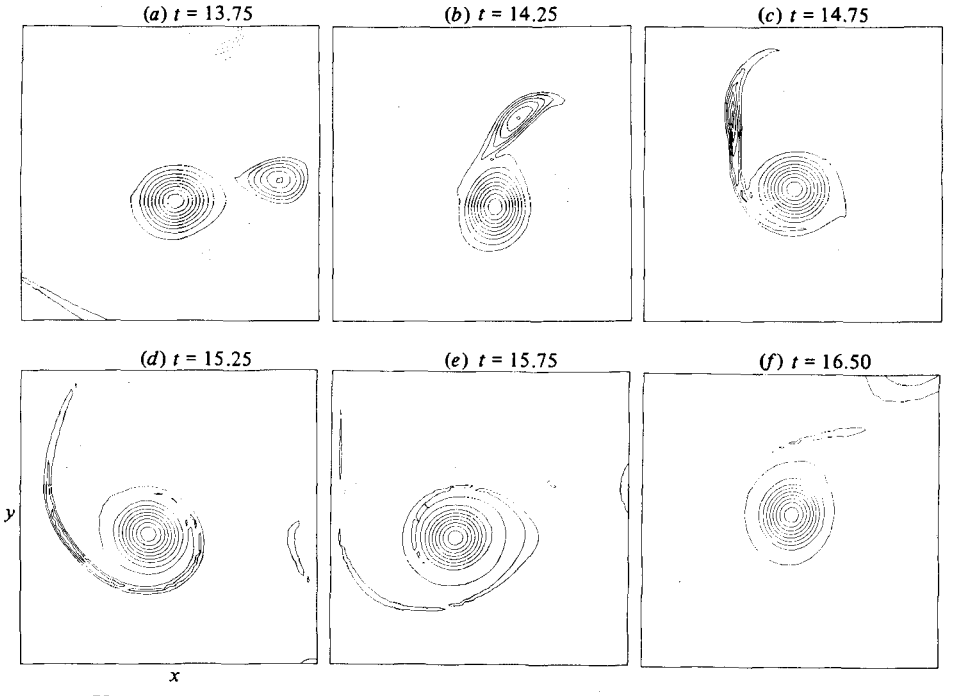

FIGURE 7. Vorticity maps in a fraction of the domain, of dimension $\frac{1}{2}\pi$, during a period of unequal-strength merger. The plotting format is as in figure 4(*b*).

extrema in vorticity, which occur by chance in locations sufficiently separated from other extrema of comparable or greater magnitude. As the turbulent cascade begins around them, the incipient vortices resist straining deformations due to neighbouring vorticity structures and grow in circulation (i.e. area-integrated vorticity) by mergers with weaker, like-sign vorticity extrema. Such unequal strength mergers yield an end-product whose extreme vorticity is bounded by the larger of the original extrema (usually that of the partner with greater circulation) and whose circulation is bounded by the sum of the original circulations. Varying amounts of the circulations, particularly that of the weaker partner, can be lost to the cascade rather than absorbed. An increase in circulation without an increase in the extremum generally implies an increase in size; thus such unequal-strength mergers are a mechanism for growth of the stronger partner.

An example of an unequal-strength merger is shown in the time sequence of vorticity maps in figure 7. Here only a small part of the circulation of the weaker partner is absorbed by the stronger; the rest is lost to the turbulent cascade. If we form a local area integral of (2) we obtain

$$\frac{\mathrm{d}C}{\mathrm{d}t} = -\oint \left[\psi \frac{\partial \zeta}{\partial s} + \nu_4 \frac{\partial}{\partial n} \nabla^2 \zeta\right] \mathrm{d}s, \tag{7}$$

where the circulation is

$$C = \iint \zeta \, \mathrm{d}x \, \mathrm{d}y. \tag{8}$$

If the boundary of the integration domain is chosen to lie outside the region of significant vorticity amplitude for the merging vortices (e.g. approximately the edges of the plots in figure 7), then the circulation of the merger end-product can be less than the initial C only if some of the vorticity is cast off, transferred to smaller scales

(so that the integrands on the right-hand side of (7) can be significant even when ζ itself is small), and advected to the boundary. Other examples of merger could be adduced that are either less or more conservative of C.

After undergoing shearing deformations or mergers, a surviving vortex will relax towards axisymmetry and a smooth radial profile, until it is again disturbed by encountering another vortex. Since vortices can only be lost through these encounters, their number will decrease with time. Vortices are lost faster than the size of the survivors grows, which implies a decrease in the number per unit area, consistent with the increasing kurtosis of figure 5. As the vortex density decreases, the frequency of encounters becomes rarer, and the rate of kurtosis increase slows. Similarly, since smaller vortices are more likely to be the weaker partner – circulation and extreme vorticity appear to be relevant measures of strength, although this must be further demonstrated – they are more likely to be destroyed in an encounter than larger vortices. Hence, for this reason as well as the growth mechanism of mergers, the average size of the survivors tends to increase. These effects of a sequence of isolated vortex interactions are illustrated by comparing vorticity patterns at different times (figure 4).

Many of the vortex encounters are non-destructive, however. Opposite-sign vortices can temporarily pair as a dipole, and like-sign vortices can circle each other, often with large structural deformations, yet subsequently separate and recover their original forms. The most common condition, though, is as an isolated, axisymmetric monopole, and this is increasingly true with time. Away from encounters with other vortices, very little time change in vorticity structure occurs, except for very slow weakening and broadening due to the small hyperviscosity. An illustration of the shape of an isolated vortex is given in figure 8.

The particular vortex selected is the one at the centre-right of figure 4(*d*). At the time plotted it has had no close encounters for 6 time units and not undergone significant deformations for 16 units. Its shape is quite close to axisymmetric and is smoothly and monotonically decreasing from the centre. There does not appear to be a unique functional form for the radial profiles of vortices; the history of interactions with other vortices seems to influence the profile (e.g. a merger between a small, intense vortex and a larger one with weaker vorticity amplitude can yield a 'breast-and-nipple' profile).

Meanwhile, an active turbulent cascade occurs in the (larger) rest of the domain outside of the isolated vortices. Vorticity structures are mutually sheared by their neighbours, and vorticity gradients increase. Energy is transferred to larger scales and enstrophy to smaller scales, where it is efficiently dissipated. Thus the vorticity that is accessible to turbulent interactions tends to disappear in time, while that which is protected in the isolated vortices persists. This yields the high kurtosis of vorticity: the isolated vortices are latent in the initial conditions and turbulence carves them out. While the turbulent component is significantly diminished with time – after all, 94 % of the original enstrophy has been lost by $t = 40$ (figure 1*b*) – it does not disappear entirely. This is illustrated in figure 9, which is simply a replotting of figure 4(*c*) with logarithmic contours to expose the weak vorticity structures between the isolated vortices. There the elongated contours have the character of the turbulent cascade (cf. figure 6).

Thus the growth in vorticity kurtosis is as much due to the cascade of the turbulent component to dissipation scales as it is to the persistence of the vortex component. Furthermore, the reduction in the kurtosis growth rate (around $t = 22$ in figure 5) coincides with the weakening of the cascade, as measured by the decreases in the amplitudes of $\mathrm{d}V/\mathrm{d}t$ and $\mathrm{d}\bar{k}/\mathrm{d}t$ in figure 1(*b*, *c*).

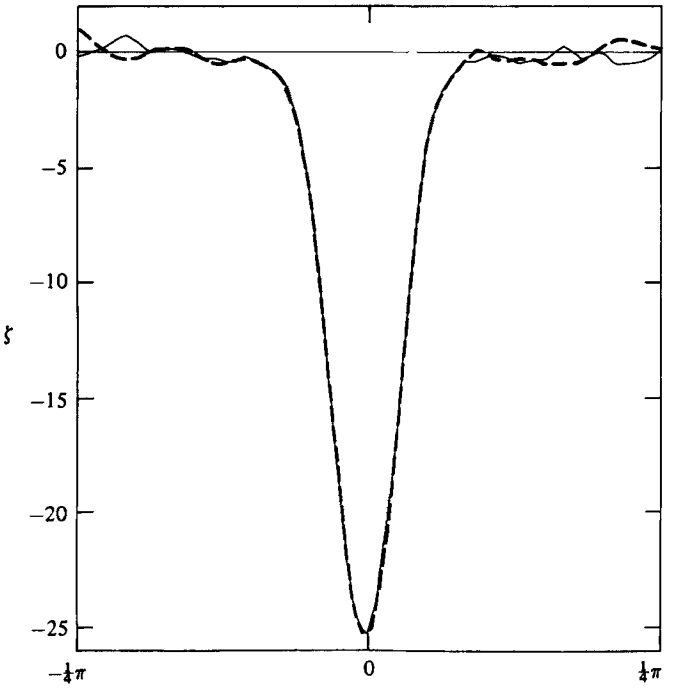

FIGURE 8. x and y cross-sections of ζ (solid and dashed lines respectively) through a vorticity minimum at $t = 40$. The abscissa is distance from the centre, where the centre is chosen to give best bulk agreement between the two profiles.

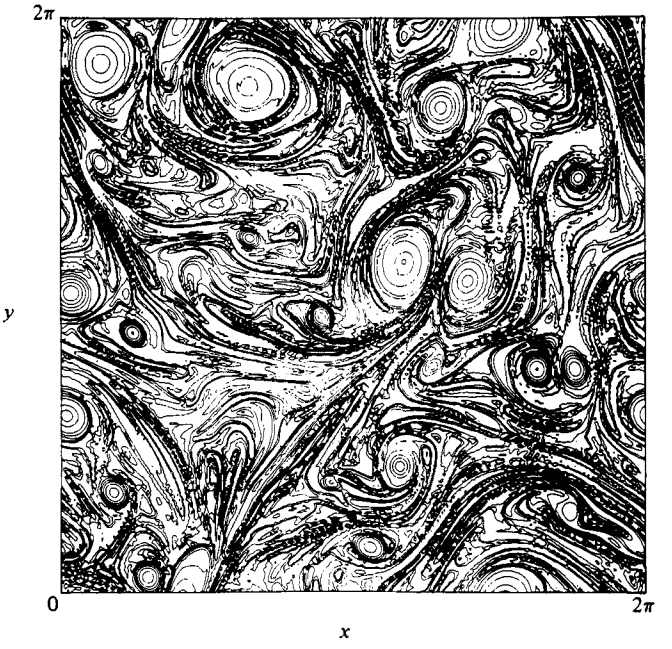

FIGURE 9. $\mathrm{Log}_{10}|\zeta|$ at $t = 16.5$ with contours every 0.25 between -0.5 and 1.5.

5. Elements of dynamical interpretation

There is considerable challenge in interpreting the phenomena described above. In this section various elements of a dynamical interpretation will be discussed, although in each case the discussion will stop short of completeness. Further studies on each of these elements would be valuable.

An important characteristic of isolated vortices is their obvious *stability*. Their long lifetimes, of course, require that even energetic perturbations not too often induce their break-up. Many studies have been made of the stability of particular vortex profiles and types of perturbations (e.g. Arnold 1980; Saffman 1980), but the full range of possibilities remains unexplored. Since a variety of profiles seem to occur in figure 4, it seems likely that many profiles are stable. A hypothesis, which I offer partly on the basis of a particular solution (Moore & Saffman 1971) and scaling arguments of F. Bretherton (personal communication), is that nearly axisymmetric vortices are robustly stable to perturbations whose strain rates and vorticity are small compared with the vorticity of the vortex. This condition is met for the flow in §3 because of the 'hard-core' character of the vorticity distribution: the scale of an individual vorticity concentration is small compared with either the typical separation between concentrations or the dominant scale of the stream function pattern.

Another dynamical process that seems to occur fairly generally is the *relaxation towards axisymmetry* of vorticity concentrations that are not initially too distorted from it. The only slowly evolving solutions of (2) are ones where isolines of ψ and ζ are parallel. In an initial configuration where this is not true one can make the hypothesis that a localized turbulent cascade will occur, carrying the non-parallel components of the vorticity to dissipation scales on a time on the order of τ_{E}. This has led to an examination of vortex solutions that have minimum enstrophy for a given energy and angular momentum or circulation (Leith 1984), where the variational principle is chosen to represent the consequences of such a local cascade. To complete the argument for relaxation to axisymmetry, one might posit that there are few, if any, distributions for a localized single-signed vorticity patch, other than axisymmetric ones, for which the isolines are parallel and which might be the end-state of a local cascade.†

Another class of dynamical questions is associated with the nature of *pairwise vortex interactions*: how many different types of interactions occur, under what conditions, and with what degree of simplicity and predictability? One important type, discussed above and illustrated in figure 7, is the merger of like-sign vortices. A number of studies have been made of idealized mergers (e.g. Christiansen 1973; Christiansen & Zabusky 1973; Overman & Zabusky 1982), but I believe we still lack a general understanding of the process, particularly with respect to how well C is conserved under various circumstances (N.B. (7)). Another important type is dipole pairing. For this we have the modon model, and some studies have been made of the dipole formation interaction (McWilliams 1983*a*) and the interaction of two dipoles (Aref 1980; Makino, Kamimura & Taniuiti 1981; McWilliams & Zabusky 1982; Larichev & Reznik 1982).

† A particular exception is an elliptical piecewise-constant vorticity solution which, in the absence of friction, simply rotates without change of shape (Lamb 1932); and generalizations of the ellipse have been found (Deem & Zabusky 1978). For such solutions the parallel-isoline requirement is non-trivial only at the boundary between the piecewise-constant regions. These solutions are probably not important exceptions to the axisymmetric selection rule, both because they are implausible end-states of a cascade and because they are inconsistent with any diffusion, in the presence of which they would probably relax to axisymmetry.

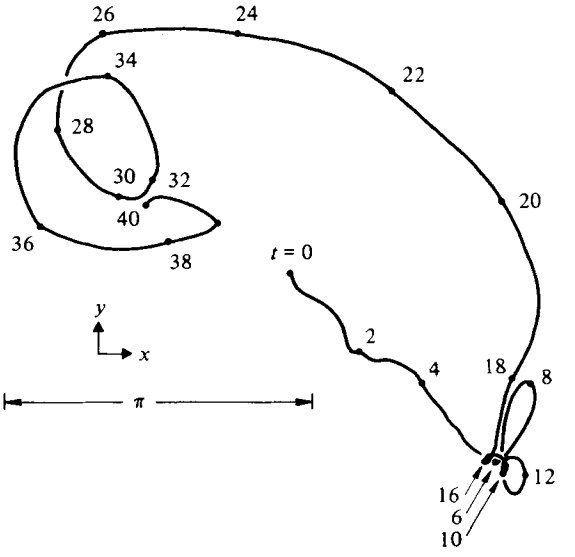

FIGURE 10. The locations of a particular vorticity maximum (the strongest one in the upper-right quadrant of figure 4(*c*) at time intervals of 0.25. Some times are labelled.

After the clear emergence of the isolated vortices from the disorderly initial vorticity distribution, which has nearly occurred by $t = 2.5$ in figure 4(*b*), a simplified characterization of the solution is that of a *finite number of point vortices*, with constant circulations and no internal degrees of freedom. Each of them is passively advected under the influence of the others. The flow is approximated as irrotational except at the points. Whenever some of the isolated vortices approach sufficiently closely, then a point-vortex approximation will be invalid since strong deformations of the vortex structures occur (i.e. internal degrees of freedom are excited), and their (generally pairwise) interaction must be calculated in detail. When sufficient separation between vortices is subsequently restored, the flow evolution again returns to that of point vortices, although possibly with a different number of vortices and with different amplitudes for those that survive the close interaction. Such an idealization of the dynamics retains the properties of chaos, and thus is turbulence of a sort. This is both because the trajectories of point vortices are in general unstable to small perturbations (Aref 1983), hence even this type of flow is chaotic, and because pairwise-isolated vortex interactions are likely to be quite sensitive to antecedent conditions as well. On the other hand it is intuitively plausible that the number of independent degrees of freedom involved in such a characterization, assuming one could usefully define them during vortex interactions, is substantially smaller than the total number of Fourier components, which is the basis for both the present numerical model and most closure theories of turbulence. Presumably this effectively diminished number of degrees of freedom has important implications for understanding the nature of the chaos and the limits of predictability of two-dimensional flows. Figure 10 gives an indication of the irregularity (chaos) in the trajectory of a particular isolated vortex which lasts throughout the integration with little change in structure (since it is the strongest extremum in the solution). Occasions of sharp change in direction are associated with close interactions with other vortices, generally of the same sign. Less-sharp changes in direction are associated with passive advection by more distant vortices. The period of particularly rapid translation

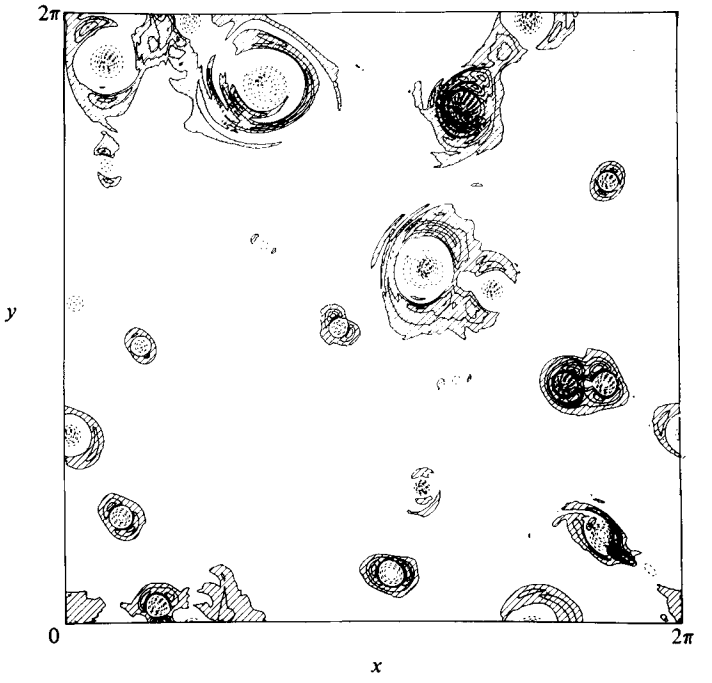

FIGURE 11. Q at $t = 16.5$. $Q < 0$ has dashed contours at an interval of 100, and $Q > 0$ has solid contours at an interval of 20, with shading within the region $Q > 20$.

between $t = 18$ and 25 is associated with a dipole pairing with an opposite-sign vortex; its curvature is a consequence of the partners being of unequal strength.

The language of §4 suggested the aptness of a *decomposition of the flow* into two components, cascading turbulence and isolated, hard-core vortices, both of which manifest chaotic behaviour, but of different types. How might this decomposition be made explicitly? One possibility is based upon the relative magnitudes of strain and vorticity (Weiss 1981). We define the two components of strain as

$$\left.\begin{aligned} S_1 &= \frac{\partial u}{\partial x} - \frac{\partial v}{\partial y} = -2\frac{\partial^2 \psi}{\partial x \partial y}, \\ S_2 &= \frac{\partial v}{\partial x} + \frac{\partial u}{\partial y} = \frac{\partial^2 \psi}{\partial x^2} - \frac{\partial^2 \psi}{\partial y^2}. \end{aligned}\right\} \tag{9}$$

Spatial differentiation of (2) and the neglect of dissipation yield

$$\frac{\mathrm{D}}{\mathrm{D}t}(\boldsymbol{\nabla}\zeta) = -\mathrm{J}(\boldsymbol{\nabla}\psi, \zeta), \tag{10}$$

where

$$\frac{\mathrm{D}}{\mathrm{D}t} \equiv \frac{\partial}{\partial t} + \mathrm{J}(\psi, \ ) \tag{11}$$

is the time derivative following a fluid parcel. If an approximation is made that both strain and vorticity are slowly varying compared with the vorticity gradient in the Lagrangian frame, then (10) has solutions of the form

$$\boldsymbol{\nabla}\zeta \propto \exp\left[\pm\tfrac{1}{2}Q^{\frac{1}{2}}t\right], \tag{12}$$

where

$$Q \equiv S_1^2 + S_2^2 - \zeta^2. \tag{13}$$

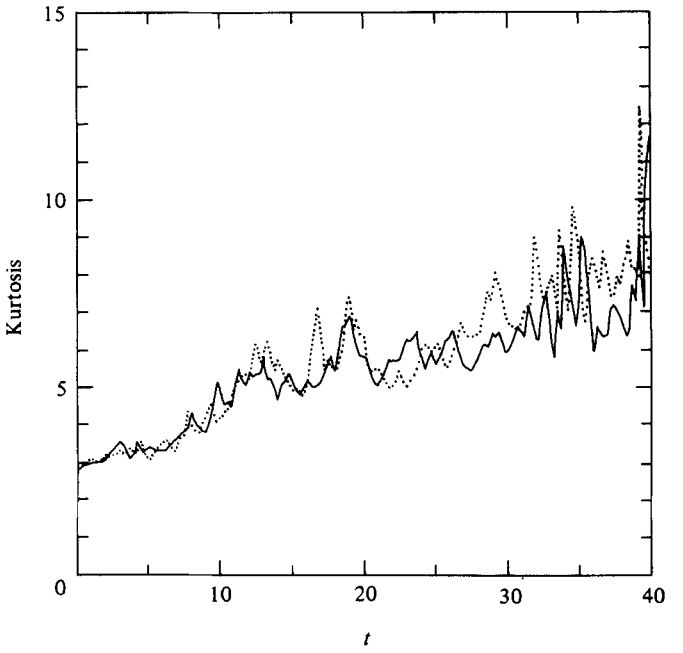

FIGURE 12. Kurtosis of the two components of strain (9). S_1 is solid and S_2 is dotted.

Thus the magnitude of the vorticity gradient will tend to grow in time at an exponential rate whenever Q is positive, and when Q is negative the time evolution is oscillatory. If we accept as an operational definition of cascading turbulence the systematic growth in vorticity gradients (N.B. the elongated contours of vorticity in figure 6), then a region with $Q > 0$ is turbulent, and one with $Q < 0$ is neutral, consistent with the persistence of vorticity patterns in isolated vortices. It can easily be shown that Q must vanish in the area integral, and furthermore that its positive and negative terms have identical vector wavenumber distributions (i.e. $\hat{S}_1^2 + \hat{S}_2^2 = \hat{\zeta}^2$, where the hat denotes Fourier transform). In spite of these identities, however, the domain is not equally partitioned into turbulent and neutral regions. This is because vorticity is more intermittently distributed than strain. This is illustrated in figure 11, where non-uniform contouring has been used to accommodate this difference. One can see that the broader $Q > 0$ regions tend to surround the $Q < 0$ regions (i.e. the isolated vortices; cf. figure 4*c*), and the strongest maxima in Q are located near strongly interacting vortices. By the preceding arguments this would imply that the most active turbulence is in the vicinity of the isolated vortices, but it is excluded from their cores. Note also that there are large regions not enclosed by either the positive or negative contours, which would suggest that much of the region is not particularly active, neither as turbulence nor persisting vortices. This is because the distribution of strain is also significantly non-Gaussian (figure 12), although much less so than vorticity (figure 5).

An alternative expression for the instantaneous tendency towards a turbulent cascade, defined as the growth of vorticity gradient, can be derived from (10); viz

$$\left.\begin{aligned} \frac{\mathrm{D}}{\mathrm{D}t}(\tfrac{1}{2}|\boldsymbol{\nabla}\zeta|^2) &= P, \\ P &\equiv \mathrm{J}(\zeta, \boldsymbol{\nabla}\psi)\cdot\boldsymbol{\nabla}\zeta. \end{aligned}\right\} \tag{14}$$

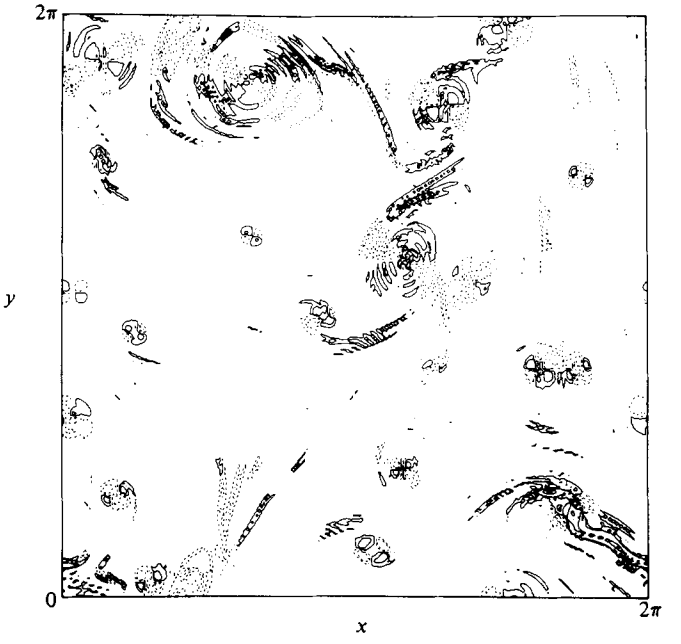

FIGURE 13. Log $|P|$ at $t = 16.5$. Contours are between 4 and 8, with an interval of 1. Positive P has solid contours and negative P has dashed ones.

This relation will be examined without any assumptions about slowly varying structure. Its spatial distribution (figure 13) is complicated. Its largest magnitudes, with both signs, again occur in the vicinity of the isolated vortices. Several features can be noted by comparing figures 4(*c*), 11 and 13.

(i) A vortex that has undergone strong deformation and is relaxing back towards axisymmetry (e.g. the negative vortex astride the top and bottom boundaries) has predominantly $P < 0$, which reflects the contracting of vorticity contours. The structure in Q (a negative region) is not particularly informative in the sense of distinguishing this particular vortex from other, more structurally inert, vortices.

(ii) The trailing streamers of vorticity in figure 4(*c*), which represent vorticity being sheared out by a stronger neighbouring vortex, are sites of active cascade, as indicated by both P and Q positive. Examples of this are the sites just above the two positive vortices in the upper-right quadrant (the upper one is just finishing the merger shown in figure 7) and the weak positive vortex just to the left of the strong positive vortex in the upper-left quadrant.

(iii) The indications of cascade are particularly strong near the two vortices in the lower-right corner, which are just beginning a merger interaction. Later they will again separate as isolated vortices, but each will have lost a substantial fraction of its circulation to the cascade.

(iv) Most of the presently non-interacting vortices, and even some that are interacting, have a quadrupole pattern in P. This indicates an alternation of stretching and contracting of vorticity contours as fluid recirculates within the vortex. Clearly this is consistent with the 'neutral' implication of $Q < 0$ and is a detailed structural tendency which appears to be lost in the slowly varying approximation. The quadrupole reflects the increase, existence, decrease, or rotation of ellipticity in an isolated vortex, depending upon the relative strength and orientation of the P-quadrupole and ζ-ellipse.

(v) There are examples of elongated, weak-amplitude vorticity structure, where P is strongly negative and Q is small: in the upper-right corner of the domain and above the contracting negative vortex in the lower left. This indicates a tendency towards formation of an axisymmetric isolated vortex. Such vortices subsequently emerge in these locations, albeit with weak amplitude and only a small fraction of the circulation evident in figure 4(*c*). Their persistence time is short because of their weakness.

(vi) In both P and Q there are substantial portions of the domain where the magnitudes are small. Together with the sparseness of the vorticity distribution, a considerable amount of spatial and temporal intermittency is indicated.

6. The generality of coherent vortices in turbulent flow

No final assessment can yet be given about how generally coherent vortices might arise in turbulent flow. However, a number of solutions have been calculated for (1), and some of the parametric influences upon the vortex component of the flow can be described.

6.1. *Friction and resolution*

Obviously, coherent vortices can neither emerge nor persist unless friction is weak; nor can turbulence. The emergence of coherent vortices does not depend qualitatively upon whether a Newtonian viscosity or hyperviscosity is used to provide the dissipation. This fact is illustrated by an alternative solution, where the hyperviscosity in (2) replaced by a Newtonian viscosity. A comparison of table 1 with figure 1 and 5 shows that the two solutions evolve similarly, with the decay rates for E, V and $\bar{k}$ slightly faster and the growth rate for $Ku(\zeta)$ slightly slower in the alternative solution. The vorticity distribution in the alternative solution is shown in figure 14 for the same time as in figure 4(*c*). The vorticity is similarly concentrated in isolated vortex cores in both cases. The vortices in the Newtonian-viscosity solution are somewhat fewer in number and slightly larger on average; these effects are consistent with the smaller effective Reynolds number for this calculation (N.B. table 2 below). However, the qualitative character of the Newtonian-viscosity solution is the same as for the hyperviscosity solution in all aspects discussed in §§3–5.

The degree to which vorticity concentrations occur is a strong function of effective Reynolds number and numerical resolution; in current practice the former is usually chosen as large as possible, given the latter, while still small enough to avoid enstrophy equipartioning (Bennett & Haidvogel 1983). This dependence is indicated in table 2, which is based upon a sequence of solutions where the resolution is doubled and the hyperviscosity is multiplied by a factor of 16 (N.B. it has units of length to the fourth power). The final member of the sequence is the one analysed above. One can see that the vorticity kurtosis is only slightly non-Gaussian at the coarsest resolution, is nearly proportional to NG for intermediate values, and seems to be levelling off at the highest resolution.

6.2. *Initial conditions*

The emergence of coherent vortices does not depend upon which realization of an initial spectrum shape (4) is taken, although the sets of vortices that emerge are different in different realizations. There is, however, a dependence upon the scale of the initial conditions in that it must be small compared with the domain size (or, as shown below, other scales that limit the inverse cascade of energy) in order for the

t	E	V	$\bar{k}$	$Ku(\zeta)$
0	0.50	138.3	8.0	3
10	0.46	13.2	2.7	15
20	0.45	7.8	2.1	23

TABLE 1. A decay solution with $\nu_2 = 10^{-4}$

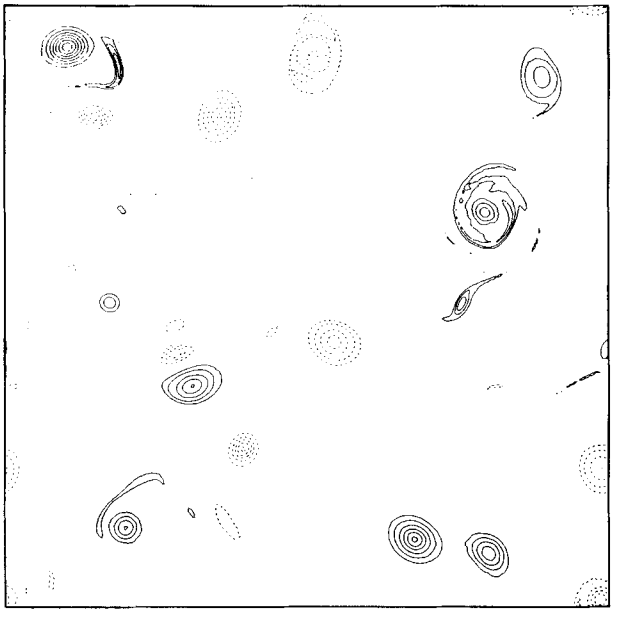

FIGURE 14. Vorticity at $t = 16.5$ for the decaying two-dimensional flow with $\nu_2 = 10^{-4}$, $\nu_4 = 0$, and other parameters as in §3. The contouring conventions are the same as in figure 4 (*b–d*).

NG	$Ku(\zeta)$ at $t = 10$
32	3.7
64	7.8
128	15.0
256	17.7

TABLE 2

vortices to emerge strongly. This is illustrated in table 3, which is based upon a sequence of calculations in which k_0 is varied in (4) (the second member of the sequence is the solution analysed above). When k_0 is not much larger than the unit domain scale, then the kurtosis is very much more slowly growing than when it is much larger. Presumably the growth of vorticity kurtosis and the emergence of coherent vortices can only occur if there is an active cascade outside the incipient vortices, and the cascade is relatively weak when k_0 is small to the degree that the finite size of the domain constrains significantly the nonlinear interactions in the flow.

For $k_0 \gg 1$ the dependence upon initial scale is weakly monotonic in both the typical vortex scale and kurtosis at long times. This is illustrated by a solution whose

	$Ku(\zeta)$	
k_0	$t = 10$	$t = 20$
2	5	9
6	18	30
18	22	30
54	20	27

TABLE 3

initial conditions contain very little energy at large scales, such that, during the vortex-emergence phase, the finite size of the domain has little consequence. The initial shape and evolution of the spectrum and the post-emergence distribution of vorticity are shown in figure 15. The coherent vortices that emerge are significantly smaller than those of the standard solution (figure 4*c*), and the inverse cascade of energy to the largest available scales has been retarded (cf. figure 2). The initial growth of vorticity kurtosis is equally rapid in the two cases. However, the reduction in kurtosis growth rate associated with the arrest of the turbulent cascade occurs at an earlier time for small-scale initial conditions (at $t \approx 7$ compared with $t \approx 22$ in figure 5). As a consequence the kurtosis at longer times is less for small-scale initial conditions: this property is seen (weakly) in table 2 for the $k_0 = 54$ solution and (more strongly) for the solution in figure 15, where $Ku(\zeta) = 23$ at $t = 20$.

6.3. *Decaying versus equilibrium solutions*

In general, larger vorticity kurtosis values seem to occur in decaying or adjusting (i.e. with rapidly changing $E(k)$) flows than in equilibrium flows, presumably because the turbulent component is constantly being replenished in the latter. Since only spatially homogeneous solutions to (1) have been calculated so far, this distinction has only been demonstrated for the temporal behaviour, but it is probably correct for the spatial behaviour as well. If, for example, forcing were confined to a small fraction of the domain, then isolated vortices might preferentially develop elsewhere.

In homogeneous equilibrium solutions one can find various degrees of coherent-vortex behaviour. In the solution of figure 6 there is no evidence of coherent vortices, and the vorticity kurtosis is approximately 3. The following parameter tendencies have been found to increase the vorticity kurtosis of the solution: slower rates for the non-conservative terms (i.e. smaller f and ν_0), more separation between the forcing and energy-containing scales, and longer correlation times in the forcing. The latter feature is incorporated by determining f from

$$\frac{\mathrm{d}f}{\mathrm{d}t} = -\frac{1}{\tau_f} f + F, \tag{15}$$

where τ_f is a correlation time for the forcing, and F is temporally white noise and spatially isotropic and band-limited in k. A particular solution, which contains all of these tendencies relative to the figure 6 solution, has equilibrium vorticity kurtosis values that vary in time between 6.5 and 10.5 and thus has a significant coherent vortex component. Its parameters are $\gamma = \beta = \nu_2 = 0$, $\nu_0 = 0.05$, $\nu_4 = 5 \times 10^{-8}$, and $\tau_f = 4$ (where $\tau_E = 1$ by either of the earlier definitions), and the forcing band limits are $k = 18.5$ and 21.5.

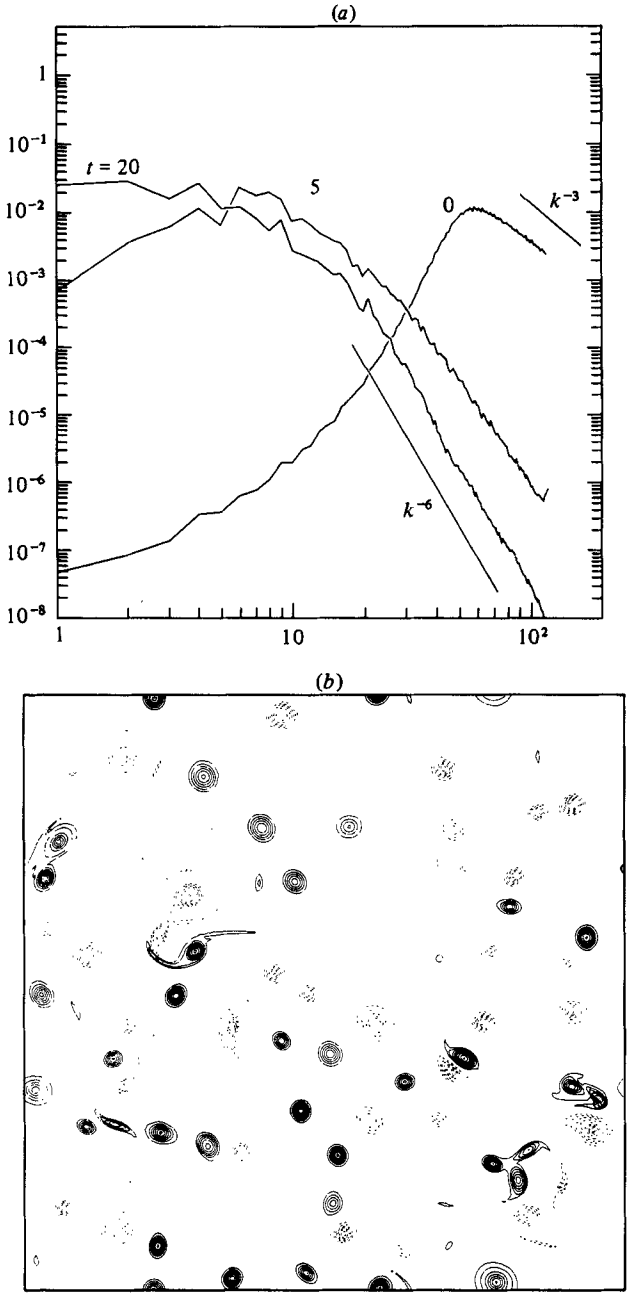

FIGURE 15. (*a*) Spectra and (*b*) vorticity for small-scale initial conditions (other parameters are as in §3). Plotting conventions are as in figures 2 and 4(*b–d*) respectively.

6.4. γ *and* β

When either of γ and β parameters is non-zero, a scale is introduced beyond which the transfer of energy by the cascade is arrested. The approximate wavenumber of this arrest is either γ or k_β, where

$$k_\beta \equiv (2E)^{-\frac{1}{4}} \beta^{\frac{1}{2}}. \tag{16}$$

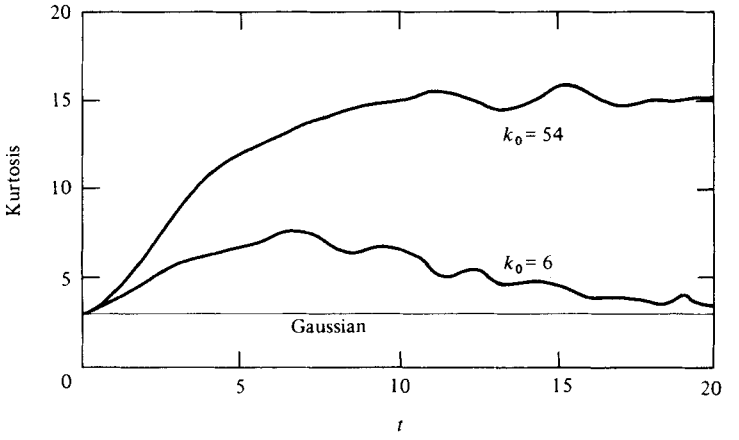

FIGURE 16. Vorticity kurtosis for two solutions of (1) with $\gamma = \nu_0 = \nu_2 = f = 0$, $\beta = 5$ and $\nu_4 = 3.125 \times 10^{-8}$.

In addition β introduces both a source of anisotropy and a wave-propagation mechanism, and in these aspects is representative of the influence of more general mean potential vorticity gradients in geostrophic turbulence (see Rhines 1979).

For finite γ the emergence of coherent vortices is about as rapid as for two-dimensional flows when $k_0 \gg \gamma$, at least for times preceding the transfer arrest, but the rate of emergence is considerably slower when this is not true (recall the similar property relative to the domain scale (§6.2)). An example of this distinction comes from two calculations with $\beta = \nu_0 = \nu_2 = f = 0$, $\gamma = 10$ and $\nu_4 = 3.125 \times 10^{-8}$: for $k_0 = 6$ the vorticity kurtosis is 4.5 at $t = 10$, whereas for $k_0 = 54$ it is 11.0.

The competition with coherent-vortex emergence is even more strenuous with β. Whenever k_0 is not too large compared with k_β, decaying flow evolves towards a state of predominantly parallel flow (i.e. $u \gg v$) when k_β is order-one or larger (Rhines 1975), and no axisymmetric coherent vortices form. On the other hand it is known that an isolated vortex, if sufficiently hard-core, can persist as a coherent entity with finite β (McWilliams & Flierl 1979). This phenomena has been demonstrated in the present context by taking the flow field from the solution of §3 at $t = 30$ (when the vortices are well developed) and using it as an initial condition in a calculation with $\beta = 5$ (i.e. $k_\beta = \sqrt{5}$): in this case the vorticity kurtosis, after an initial drop (due to advection of particles in the initially irrotational region between the vortices), remains large and the vortices persist. In contrast, if the initial condition is a random field of the same type as for the §3 solution (i.e. with $k_0 = 6$), the kurtosis approaches the Gaussian value at intermediate times (figure 16). At early times when the flow is adjusting and the cascade is active, there is a spurt in the kurtosis as vortices begin to emerge; however, they are not sufficiently well developed by the time of the transfer arrest and subsequently collapse. If the initial scales are sufficiently small, though, then the vortices will be strong enough at the time of the arrest to endure (see the $k_0 = 54$ curve in figure 16). Thus coherent vortices can emerge from random initial conditions when $k_0 \gg k_\beta$.

The inhibiting effect of β on vortex emergence also has been discussed recently by Holloway (1983).

7. Discussion

A variety of examples have been presented of the emergence and persistence of isolated concentrations of vorticity in turbulence flows. These constitute a *prima facie* case for the considerable commonness of the occurrence, though not ubiquity, of this phenomenon. This phenomenon also requires a substantial extension of extant characterizations of two-dimensional and geostrophic turbulence. In particular, higher-moment closure theories (e.g. Kraichnan 1971) have been developed without reference to such vorticity concentrations (nor to the extremely non-Gaussian distributions associated with them), and the question now arises whether they will be accurate in predicting the second-moment quantities for which they were developed, such as the spectrum, in circumstances where the vorticity is strongly concentrated. Herring & McWilliams (1984) have shown that, for some of the solutions presented in this paper, comparable closure solutions do indeed have some significant differences in second-moment quantities. Much of our present interpretation of atmospheric predictability limits is based upon such closure-theory solutions (Leith 1971; Leith & Kraichnan 1972), and the possibility of long-lived vortices may alter the interpretation.

There are perhaps several reasons why so little has been made of coherent vortices in the many previous numerical calculations of two-dimensional turbulence. Not the least of these reasons, I suspect, is simply the lack of an *a priori* concern with this issue by the investigators, whereas I began the present study specifically with the question of the survival of vortices in turbulence in mind. Other factors are the lower resolutions (lower Reynolds numbers) and shorter integration times of previous studies, both of which diminish the coherent-vortex component of the solution (§6). In retrospect, however, it is easy to see manifestations of the vortices in some of the earlier solutions, some of which were noted by the investigators but not given the present emphasis (Fornberg 1977; Basdevant *et al.* 1981).

There are several other circumstances, beside the ones discussed above, where isolated vortices in turbulent flow have been reported. Among these are the spatial concentration of vorticity in a numerical calculation of a two-dimensional shear layer (Aref & Siggia 1980), isolated vortices in irregularly forced flow in rotating laboratory tanks (McEwan 1976; Hopfinger, Browand & Gagne 1982), and long-lived axisymmetric ocean eddies on scales somewhat smaller than the most energetic currents (McWilliams *et al.* 1983). The laboratory vortices exhibit a strong asymmetry in vortex parity, where those with vorticity of the same sign as the background rotation are much stronger than those with opposite sign. Since both the forcing and the two-dimensional equations are symmetric with respect to vortex parity, the observed asymmetry must be due to three-dimensional ageostrophic components of the flow. The ocean eddies have three-dimensionally concentrated vorticity, and an interpretation of them as analogous to the present solutions requires a generalization of the two-dimensional vortex phenomenon to fully three-dimensional geostrophic turbulence; this analogy has been argued on general (not vortex-specific) grounds by Charney (1971). At present I do not feel it warranted to claim any close identification between the present solutions and these other phenomena, although the possibility obviously exists.

If there are geophysical counterparts of the isolated vortices shown here, they should occur on scales not large compared with k_β^{-1} and γ^{-1}. In the midlatitude atmosphere and ocean, this implies upper bounds on horizontal scale of orders 1000 km and 100 km respectively. Furthermore, if they are to arise from irregular forcing (e.g.

flow over topography, thermal convection), the forcing scale should be small compared with these bounds, in order that the vorticity concentration mechanism have sufficient time to operate before an arrest of the turbulent cascade occurs.

During the course of this investigation I have benefited from conversations with F. Bretherton, D. Haidvogel (whose model I used), J. Herring, G. Holloway, R. Kraichnan, C. Leith and N. Zabusky. Programming support was provided by J. Chow and N. Norton. The work was sponsored by the National Science Foundation through its support of the National Center for Atmospheric Research. A preliminary report of this work was presented at a conference on the Predictability of Fluid Flow sponsored by the La Jolla Institute, La Jolla, California (McWilliams 1983*b*).

REFERENCES

Aref, H. 1980 Coherent features by the method of point vortices. *WHOI Tech. Rep.* 80–53, pp. 233–249.

Aref, H. 1983 Integrable chaotic and turbulent vortex motion in two-dimensional flows. *Ann. Rev. Fluid Mech.* **15**, 345–389.

Aref, H. & Siggia, E. 1980 Vortex dynamics of the two-dimensional turbulent shear layer. *J. Fluid Mech.* **100**, 705–737.

Arnold, V. I. 1980 *Mathematical Methods of Classical Mechanics.* Springer.

Basdevant, C., Legras, B., Sadourny, R. & Beland, M. 1981 A study of barotropic model flows: intermittency, waves and predictability. *J. Atmos. Sci.* **38**, 2305–2326.

Batchelor, G. K. 1953 *The Theory of Homogeneous Turbulence.* Cambridge University Press.

Batchelor, G. K. 1969 Computation of the energy spectrum in homogeneous two-dimensional turbulence. *Phys. Fluids Suppl.* **12**, II-233–II-239.

Bennett, A. F. & Haidvogel, D. B. 1983 Low resolution numerical simulation of decaying two-dimensional turbulence. *J. Atmos. Sci.* **40**, 738–748.

Charney, J. G. 1971 Geostrophic turbulence. *J. Atmos. Sci.* **28**, 1087–1095.

Christiansen, J. P. 1973 Numerical simulation of hydrodynamics by the method of point vortices. *J. Comp. Phys.* **13**, 363–379.

Christiansen, J. P. & Zabusky, N. J. 1973 Instability, coalescence and fission of finite-area vortex structures. *J. Fluid Mech.* **61**, 219–243.

Davey, M. K. 1980 Numerical calculation of the spectral representation of $\boldsymbol{u}\cdot\boldsymbol{\nabla}_x$ for doubly periodic flow. *Univ. Washington Special Rep.* 93.

Deem, G. S. & Zabusky, N. J. 1978 Vortex waves: stationary V-states, interactions, recurrence and breaking. *Phys. Rev. Lett.* **40**, 859–862.

Fornberg, B. 1977 A numerical study of 2-D turbulence. *J. Comp. Phys.* **25**, 1–31.

Haidvogel, D. B. 1983 Particle dispersal and Lagrangian vorticity conservation in models of β-plane turbulence. In preparation.

Herring, J. & McWilliams, J. C. 1984 Comparison of direct numerical simulation of two-dimensional turbulence with two-point closure. Submitted.

Holloway, G. 1983 Contrary roles of planetary wave advection in atmospheric predictability. In *Proc. La Jolla Conf. on Predictability* (ed. G. Holloway & B. West). *AIP Conf. Proc. no.* 106, pp. 593–599.

Hopfinger, E., Browand, F. & Gagne, Y. 1982 *J. Fluid Mech.* **125**, 505–534.

Kraichnan, R. H. 1971 An almost-Markovian Galilean-invariant turbulence model. *J. Fluid Mech.* **47**, 513–524.

Kraichnan, R. H. & Montgomery, D. 1980 Two-dimensional turbulence. *Rep. Prog. Phys.* **00**, 000–000.

Lamb, H. 1932 *Hydrodynamics*, 6th edn, §159. Dover.

Larichev, V. & Reznik, G. 1982 Numerical experimental studies of interactions between dimensional elongated Rossby waves. *Rep. Acad. Sci. USSR, Oceanologie* **264**, 229–233.

LEITH, C. E. 1971 Atmospheric predictability and two-dimensional turbulence. *J. Atmos. Sci.* **28**, 145–161.

LEITH, C. E. 1984 Minimum enstrophy vortices. *Phys. Fluids* in press.

LEITH, C. E. & KRAICHNAN, R. 1972 Pedictability of turbulent flows. *J. Atmos. Sci.* **29**, 1041–1058.

MCEWAN, A. 1976 Angular momentum diffusion and the initiation of cyclones. *Nature* **260**, 126–128.

MCWILLIAMS, J. C. 1983*a* Interactions of isolated vortices. II. Modon generation by monopole collision. *Geophys. Astrophys. Fluid Dyn.* **24**, 1–22.

MCWILLIAMS, J. C. 1983*b* On the emergence of isolated, coherent vortices in turbulent flow. In *Proc. La Jolla Conf. on Predictability* (ed. G. Holloway & B. West). *AIP Conf. Proc. no.* 106, pp. 205–221.

MCWILLIAMS, J. C. *et al.* 1983 The local dynamics of eddies in the Western North Atlantic. In *Eddies and Marine Science* (ed. A. Robinson), pp. 92–113. Springer.

MCWILLIAMS, J. C. & FLIERL, G. R. 1979 On the evolution of isolated, nonlinear vortices. *J. Phys. Oceanogr.* **9**, 1155–1182.

MCWILLIAMS, J. C., FLIERL, G. R., LARICHEV, V. D. & REZNIK, G. M. 1981 Numerical studies of barotropic modons. *Dyn. Atmos. Oceans* **5**, 219–238.

MCWILLIAMS, J. C. & ZABUSKY, N. J. 1982 Interactions of isolated vortices. I. Modons colliding with modons. *Geophys. Astrophys. Fluid Dyn.* **19**, 207.

MAKINO, M., KAMIMURA, T. & TANIUITI, T. 1981 Dynamics of two-dimensional solitary vortices in a low-β plasma with convective motion. *J. Phys. Soc. Japan* **50**, 980–989.

MALANOTTI-RIZZOLI, P. 1982 Planetary waves in geophysical flows. *Adv. Geophys.* **24**, 147–224.

MOORE, D. W. & SAFFMAN, P. G. 1971 In *Aircraft Wake Turbulence* (ed. J. H. Olsen, A. Goldberg & M. Rogers), pp. 339–000. Plenum.

OVERMAN, E. A. & ZABUSKY, N. J. 1982 Evolution and merger of isolated vortex structures. *Phys. Fluids* **25**, 1297–1305.

RHINES, P. B. 1975 Waves and turbulence on a beta-plane. *J. Fluid Mech.* **69**, 417–443.

RHINES, P. B. 1979 Geostrophic turbulence. *Ann. Rev. Fluid Mech.* **11**, 401–441.

SAFFMAN, P. G. 1980 In *Transition and Turbulence* (ed. J. H. Olsen, A. Goldberg & M. Rogers), pp. 339–000. Plenum.

WEISS, J. 1981 The dynamics of enstrophy transfer in two-dimensional hydrodynamics. *La Jolla Inst.* LJI-TN-81-121.